Accepted Manuscript

Factory-on-chip: Modularised microfluidic reactors for continuous mass production of functional materials [$]

Tengteng Han, Li Zhang, Hong Xu, Jin Xuan

PII: S1385-8947(17)30979-8
DOI: http://dx.doi.org/10.1016/j.cej.2017.06.028
Reference: CEJ 17109

To appear in: *Chemical Engineering Journal*

Received Date: 16 December 2016
Revised Date: 2 June 2017
Accepted Date: 5 June 2017

Please cite this article as: T. Han, L. Zhang, H. Xu, J. Xuan, Factory-on-chip: Modularised microfluidic reactors for continuous mass production of functional materials [$], *Chemical Engineering Journal* (2017), doi: http://dx.doi.org/10.1016/j.cej.2017.06.028

Factory-on-chip: Modularised microfluidic reactors for continuous mass production of functional materials [$]

Tengteng Han [1], Li Zhang [1, 3*], Hong Xu [1,3], Jin Xuan [2,*]

[1] State-Key Laboratory of Chemical Engineering, School of Mechanical and Power Engineering, East China University of Science and Technology, Shanghai, 200237, China

[2] School of Engineering and Physical Sciences, Heriot-Watt University, Edinburgh, EH14 4AS, United Kingdom

[3] Shanghai Institute of Materials Genome, Shanghai, 200237, China

*Corresponding Authors, Tel: +44 (0) 131 451 3293; Fax: +44 (0)131 451 3129, Email addresses: j.xuan@hw.ac.uk (J. Xuan); Tel: +86 21-64252847, Email addresses: lzhang@ecust.edu.cn (L. Zhang).

[$] Electronic Supporting Information is available

Highlights

1. Factory-on-chip concept is demonstrated with multi-dimensional scale-up strategy.

2. Design principle is derived with the flow resistance model of a 3D microfluidic flow network.

3. A module with 80 channels is fabricated and investigated with two fluid systems.

4. Chitosan/TiO_2 composite material is continuously synthesized and characterized.

Graphical Abstract

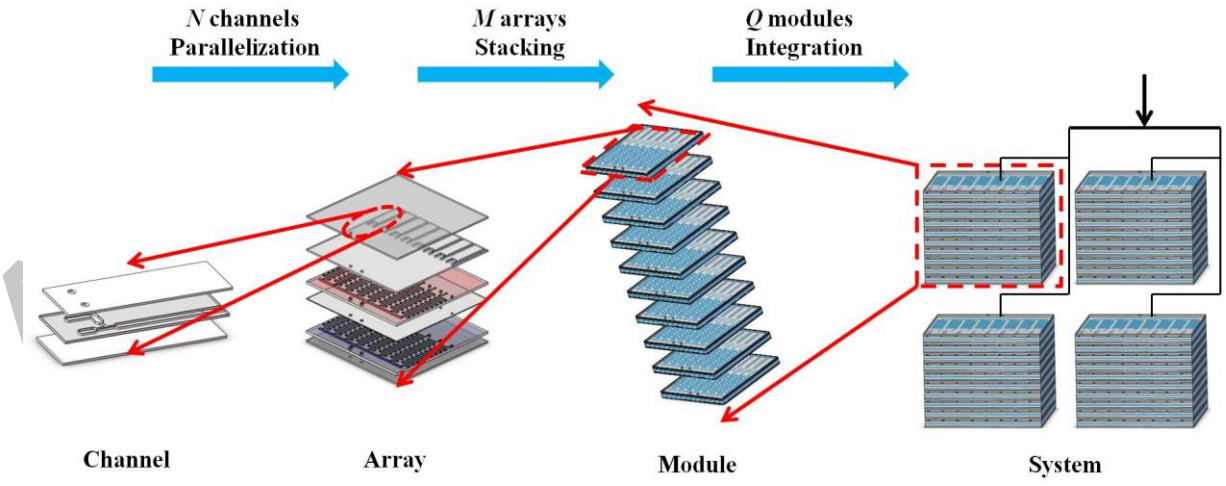

Abstract

Droplet microfluidics provide an advanced platform for functional material synthesis. However, the process has been largely limited to the scale of laboratory study with the device known as lab-on-chip. Here, a multi-dimensional scale-up strategy based on modularised microfluidic reactors is presented to develop large-scale devices defined as factory-on-chip, achieving throughput enhancement to the industrial production scale. Under the guidance of the derived principle, an up-scaling system is demonstrated with eight microchannels parallelized to form an array, ten arrays stacked as the module, and five modules integrated in a system with 400 channels in total. Experiments showed that the circular array arrangement improved the uniformity of product droplets by 42.4% compared to that achieved with a parallel array. The stacking effect was also investigated with two types of material production systems. Chitosan/TiO_2 composite microspheres, as advanced wastewater treatment material, were continuously synthesized in mass production with a narrow size distribution of 3.59%, which could hardly be achieved with conventional methods. The material exhibited a methyl-orange dye removal efficiency of 65.3%, which constitutes an improvement of 10.8% compared to single-component chitosan microspheres.

Keywords: Microfluidics; Microreactors; Scale-up; Factory-on-chip; Continuous synthesis

1 Introduction

Micro-scale technology and engineering have been attracting much attention from chemical engineers for decades owing to the advantages of efficient fluid handling, continuous operation, process intensification, and excellent product performance [1].

Droplet-based microfluidics is a promising micro-technology for advanced material synthesis. It provides a powerful platform allowing the generation of droplet/particle functional materials with high controllability and uniformity [2-6], which is not possible with conventional methods. Functional materials synthesized from microfluidics have a wide range of applications in chemical fields [7-8]. In addition, microchannel parallelization is an effective integration method for scale-up without the amplification effect, and it has great prospects for future development [9].

Thus far, the research efforts on microfluidics have been mostly limited to the lab-on-chip concept for better control of the compositions, morphologies, and microstructures of various materials, while ignoring the low throughput generated from individual microchannels which hinders industrial applications. To address this challenge, it is highly desired to investigate microfluidic up-scaling technology to realize the factory-on-chip concept, i.e., a factory integrated and built on small chips with an industrial-scale production rate while maintaining excellent controllability and highly efficiency.

Larger-scale microfluidic devices have been reported for the mass production of droplets/materials in the literature [10-19]. Nisisako et al. first reported the production of monodisperse single and compound droplets with a glass lab-on-chip parallelizing 256 channels arranged circularly to achieve large-scale production [10]. Similarly, Issadore et al. and Lee et al. parallelized 1000 and 512 channels in PDMS to achieve a throughput of 0.028 L/h and 1.5 L/h, respectively [15, 17]. The above studies investigated scale-up technology with a two-dimensional array, while three-dimensional stacking devices with channels parallelized in the vertical direction were achieved using 512 channels of PMMA and 28

channels of photoresist, with volumetric production rates of 1 L/h and 3 L/h, respectively, which is the highest rate reported to date [16,18]. The modular concept was also applied for further scale-up with each module working independently. Kumacheva et al. integrated eight modules with each consisting of sixteen channels [11], and the Telos® system integrating ten modules developed by Dolomite Company (the United Kingdom) made the first attempt to achieve successful commercial transition.

To date, an effective systematic scale-up strategy suitable for the industrialization of microfluidic technology is still not available. In two-dimensional arrays, the parallelization of more channels will lead to a high pressure imbalance among branches, resulting in polydispersity and thereby low-quality products. Therefore, the number of parallelized channels forming an array is limited. Moreover, no design principle has yet been developed to guide three-dimensional microfluidic network design, except for the two-dimensional array design rules that were posited and validated by Issaore et al, Lee et al, and Weitz et al [13, 15, 17]. In addition, in all the above studies, channels with size of the order of tens of microns were fabricated with high accuracy but high risk of channel blockage, which could hardly meet real-world requirements from a chemical engineering perspective, even with a large number of channels. To address these challenges, a multi-dimensional scale-up strategy based on modularised stacks is present to meet industrial requirements. The concept is depicted in Fig. 1. Specifically, to scale up, *N* microchannels are parallelized on a two-dimensional array, and *M* arrays are stacked in a reconfigurable manner in the third dimension as a module. The integration of *Q* modules could achieve a production rate proportional to three scale-up numbers *N*, *M*, and *Q*.

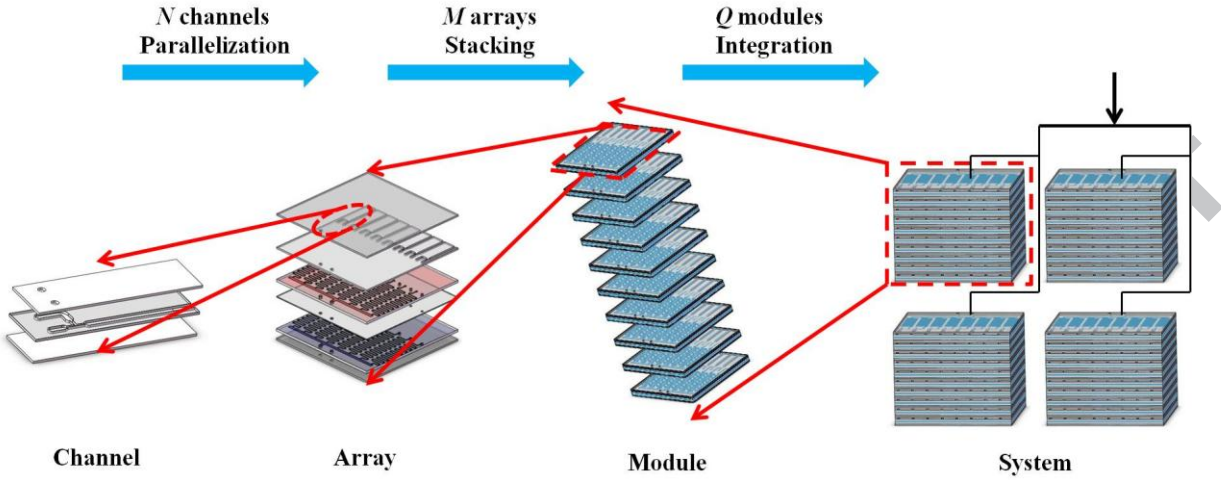

Fig. 1 Overview of multi-dimensional scale-up strategy (not to scale).

In this study, the process design principle for a three-dimensional microfluidic network is derived to distinguish the inherent relationship among scale-up numbers, product uniformity, and channel design parameters. With the design principle for guidance, eight microchannels were parallelized in each array, ten arrays were stacked in the vertical direction as a module, and five modules were integrated in a microfluidic system consisting of 400 channels in total to mass-produce monodispersed droplets/particles. The parallelization effect and stacking effect were both investigated and discussed with two different types of fluid systems. Chitosan/TiO_2 composite functional materials were mass-synthesized and characterized. Such material is chosen because Chitosan is a promising and competitive alternative as a green adsorbent for the treatment of polluted wastewater containing dyestuff and heavy metals owing to its biocompatibility, biodegradability, and non-toxicity [20, 21]. Our research team has demonstrated the higher and excellent adsorption capacity for methyl orange of single-chitosan microspheres under microfluidics [22]. To further improve the dye removal performance, Chitosan microparticle modification is a promising approach. Nano-TiO_2 has

been used for the photocatalytic treatment of wastewater, but it is easily drained and difficult to recover [23]. Therefore, a Chitosan/TiO2 composite material could have advantages from both materials and show promising in the water treatment applications [24].

2 Methodology

2.1 Flow resistance model

A flow resistance model was developed to study the effect of the flow resistance along neighbouring channels inputs (R_f), the resistance of each channel (R_u), the equivalent resistance of a single array from input to output (R_c), the flow resistance of the vertical channel among neighbouring arrays (R_v), and the motivation under a gravity field (R_g), as shown in Fig. 2. To achieve a three-dimensional microfluidic network with uniform distribution, R_u must be significantly greater than R_f. Meanwhile, R_c should be significantly greater than the absolute difference between R_v and R_g. The design principle will be derived based on the flow resistance model and the criteria described above.

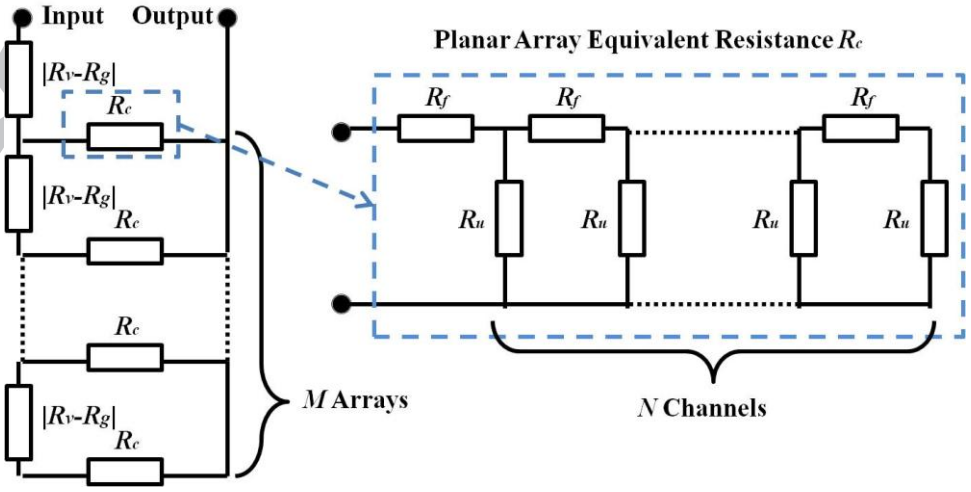

Fig. 2 Model for the hydraulic resistance of a three-dimensional microfluidic network.

2.2 Reactor module design and fabrication

Two different types of arrays, i.e., parallel and circular arrays with eight channels, were designed. Fig. 3 shows the parallel array configuration and stacking assembly. The array is composed of six basic layers of 80 mm × 80 mm area, stacked and bonded on top of each other. The fluid distributions for two phases have long serpentine pathways as flow resistors so that a uniform distribution is achieved. Two additional through-holes were designed next to the edge of the layers to connect distribution channels of distribution layers, forming the vertical distribution channel of the modularised stack. Similarly, the circular array also consists of three main layers. The only difference among the two arrays is in the phase distribution layer, where the distribution area was transformed from side rectangular to central reservoir.

Ten arrays were assembled as a module with a common fluid input, allowing for the reduction of pump consumption and connecting tubes. These arrays were stacked on top of each other with the alignment of through-holes that were fabricated along the edge, forming the vertical distribution channel to deliver fluid to each array. The first/top array was connected to pumps, and the last/bottom array to a dead stop.

Polymethylmethacrylate (PMMA) was chosen as the substrate because of its strength after bonding, capability of withstanding high pressures, and long lifespan. The fabrication process consists of laser microfabrication engraving (Universal VLS2.30) and thermo-compression bonding. The microchannel engraving is cost-effective and does not require a clean room facility. After the completion of all six layers, thermal-compression bonding was applied to seal these six PMMA layers together to form enclosed channels under

the set pressure and temperature conditions of 0.2 MPa and 100℃, respectively. Ten arrays were stacked on top of each other and glued by UV-curing adhesive to form the module.

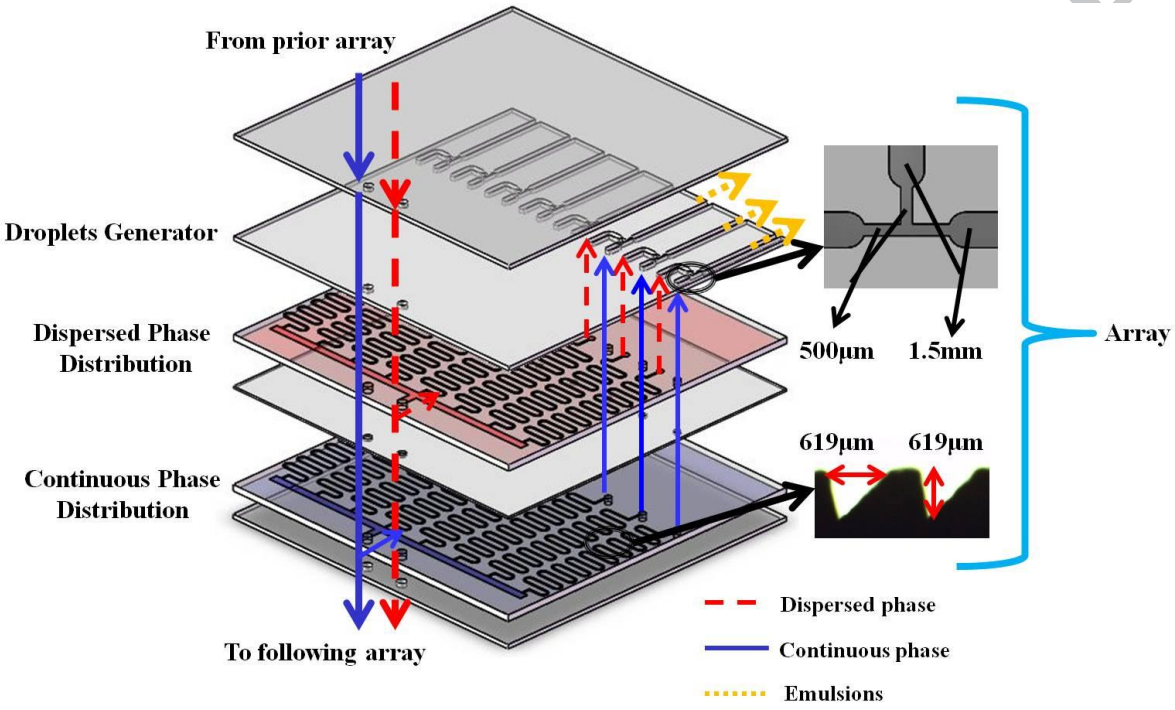

Fig. 3 Microfluidic module design. Parallel array configuration and stack assembly is depicted. The individual array consists of six layers of 80 mm × 80 mm area. The serpentine passages are small triangular sections with a size of 619 μm, and a cross-sectional view under an optical microscope is presented.

2.3 System operation

Two fluid systems were used for experiments. In the first operation to produce water-in-oil droplet products, octane (≥96%) with 8% Span80 added as a surfactant and deionized water coloured with methyl orange were used as the continuous and dispersed phase, respectively. In the second experiment to synthesize a chitosan/TiO_2 functional

material for photocatalysis and adsorption, the material is the same as in the preparation of single chitosan microspheres reported by our research team [22], except for the dispersed phase, where 0.35 wt% TiO_2 powder was added to improve adsorption capacity, taking advantage of the photocatalytic degradation of nanometre-scale TiO_2.

Fig. 4 shows the experimental system. A pressure controller containing fifteen independently controlled outputs (WH-PMPP-15, Wenhao Co., Ltd., SuZhou, China) was used for driving the fluid. Each module requires two outputs, and each output allows independent control, which enables the independent operation of modules without interrupting other modules.

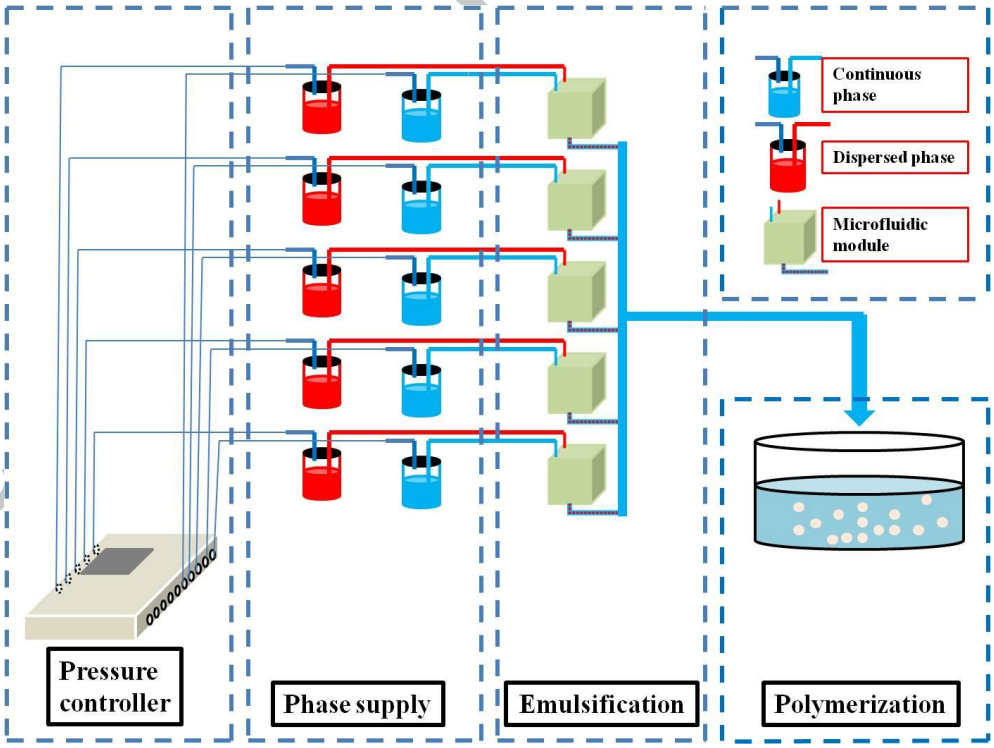

Fig. 4 Overall schematic of the experimental system integrating five modules.

2.4 Material Characterisation

The droplets and chitosan/TiO_2 composite microspheres were observed using an optical microscope with a digital camera (OLYMPUS SZX7) and a scanning electron microscope (JEOL JSM-6380LV). Approximately 200 droplets or/and microspheres were measured each time and analysed yielding a mean diameter and monodispersity defined using the coefficient of variance (CV).

The Chitosan/TiO_2 composite microspheres with the multi-functional performance of adsorption and photocatalytic degradation have a wide range of applications with a strengthening treatment effect for industrial wastewater containing toxic organic compounds, heavy metals, etc. [24, 25]. In this study, methyl orange (MO) dye adsorption was taken as an example to characterize the newly designed material. Batch adsorption experiments were conducted for comparison. For each group of experiments, 5 mg chitosan microspheres, 5 mg TiO_2 powder, and 5 mg chitosan/TiO_2 composite material were added, respectively, to 25 mL MO solution prepared with a concentration of 60 mg/L. The experiments were conducted at room temperature under continuous shaking and exposure to UV-Vis light of 365-nm wavelength with 100% amplitude [22]. At given time intervals of 1, 1.5, 2, 2.5, 3, 4, 5, 6, 7, and 8 h, the residual concentration was determined from a calibration curve constructed by measuring the absorbance at 465 nm using UV-Vis spectroscopy (Xin Mao Instrument, UV-7502). Each experiment was repeated 5 times, and the average value was considered. The adsorption efficiency (η) was calculated according to the following equation [22]:

$$\eta(\%) = \frac{(C_0 - C_t)}{C_0} \times 100\%, \quad (1)$$

where C_0 is the initial concentration of MO (mg/L) and C_t is the instantaneous concentration

of MO at a predetermined time *t*.

3 Results and discussion

3.1 Design principle

The design principle of the two-dimensional array has been posited and validated to achieve a uniform distribution in the ladder geometry [13, 15, 17]:

$$2N\left(R_f / R_u\right) \le 0.01 \quad (2)$$

In order to reveal the inherent relationship among scale-up numbers, flow uniformity, and microchannel design parameters, in this study, the equation 2 was modified as equation 3 and equation 4 for array and stack design based on resistance model depicted in Fig. 2:

$$N\left(R_f / R_u\right) = \delta, \quad (3)$$

$$M\left(\left|R_v - R_g\right| / R_c\right) = \beta, \quad (4)$$

where N is the number of channels in the array and M is the number of arrays stacked as the module. δ and β are numbers that indicate the fluid distribution uniformity. Smaller δ and β values indicate higher uniformity. In general, δ or β should be less than 0.005 to achieve relatively acceptable uniform fluid delivery in the three-dimensional microfluidic network [13, 15, 17]. R_i (where i could be u, v, g) is the corresponding laminar flow resistance of the three-dimensional network, determined by the channel size and length and the viscosity of the fluid system and is estimated using equation 5 based on basic fluid mechanics:

$$R_i = \frac{128\mu L}{\pi D_h^{\,4}}. \quad (5)$$

The equivalent resistance R_c of a single array from input to output is calculated based on the

resistance model based on mathematical methods with equation 3:

$$R_{c,N} = \left[\frac{\delta/N}{2} + \left(\frac{g^N(\delta/N)+1}{g^N(\delta/N)-1} \right) \frac{\sqrt{(\delta/N)^2 + 4\delta/N}}{2} \right] R_u , \quad (6)$$

where $g(\delta/N) = \dfrac{\delta/N + 2 + \sqrt{(\delta/N)^2 + 4\delta/N}}{\delta/N + 2 - \sqrt{(\delta/N)^2 + 4\delta/N}}$.

$R_{c,N} = f(\delta/N, N)R_u$, and $f(\delta/N, N)$ is defined as equivalent resistance coefficient of the array. $R_{c,N}$ is mainly affected by R_u and the parallelization number N, and a higher R_u results in a higher R_c. However, increasing N will lead to a smaller R_c, making it more difficult to achieve a uniform vertical distribution. Therefore, the stacking number M is limited. To satisfy equations 3 and 4, serpentine pathways were utilized as flow resistors [26]. The improved flow uniformity with serpentine pathways can be explained through an electronic-hydraulic analogy [27-29]. According to the correlation derived from Hagen-Poiseuille's law (equation 7), the hydraulic resistance of serpentine pathways is high with high viscosity, long length and narrow cross-sectional area [29]. Therefore, long pathways approximately 280 mm in length with a size of 619 μm were designed. Considering the equipment size, eight channels were parallelized on a PMMA sheet of 80 mm × 80 mm area. Based on the design constraint and these flow-resistance estimations with N = 8, we determined that M should less than 11 when δ and β are set to 0.005. Therefore, N = 8 and M = 10 are selected for the module design and scale-up experiment.

$$\tau = \frac{\mu L \chi}{2\pi A} \quad (7)$$

From equations 3, 4, and 6, the design principle of the array and stack is integrated to obtain the three-dimensional microfluidic network design principle, as expressed by equation

8, to give guidance for stack design, where $K_R = \frac{|R_v - R_g|}{R_u}$ is defined as the design parameter of the stack/module.

$$\frac{K_R}{\beta/M} = f\left(\delta/N, N\right), \tag{8}$$

For single two-dimensional parallelization (see equation 3) with fixed-sized channels, greater channel parallelization results in a higher δ. In other words, droplet uniformity worsens with increasing number of channels with a fixed slope of K_1. Therefore, the parallelization number N should be limited to obtain more uniform droplets, reflecting the limitation of two-dimensional parallelization. This drawback can be overcome by the multi-dimensional scale-up strategy, where the throughput could be substantially scaled up without excessively sacrificing droplet uniformity. The stacking procedure arrests the worsening of uniformity with an adjustable slope K_2 determined by counteraction of R_v and R_g. Furthermore, the K_2 value (equation 10) should be smaller than K_1 (equation 9) to utilize the advantage of the stacking procedure, which is easy to be achieved. The integration of modules with independent control theoretically has little influence on the uniformity of droplets. Here, a fixed slope of K_3 is defined to reflect the droplet uniformity worsen with increasing number of modules in the system due to manufacturing and system operation errors in practical cases. Specifically, the comparison result of multi-dimensional scale-up strategy (8×10×5) and two-dimensional parallelization with a total of 400 channels is depicted in Fig. 5. It demonstrates the great advantage of our multi-dimensional scale-up strategy.

$$K_1 = R_f / R_u, \tag{9}$$

$$K_2 = \frac{\left|R_v - R_g\right|}{f(K_1,8)R_u}. \tag{10}$$

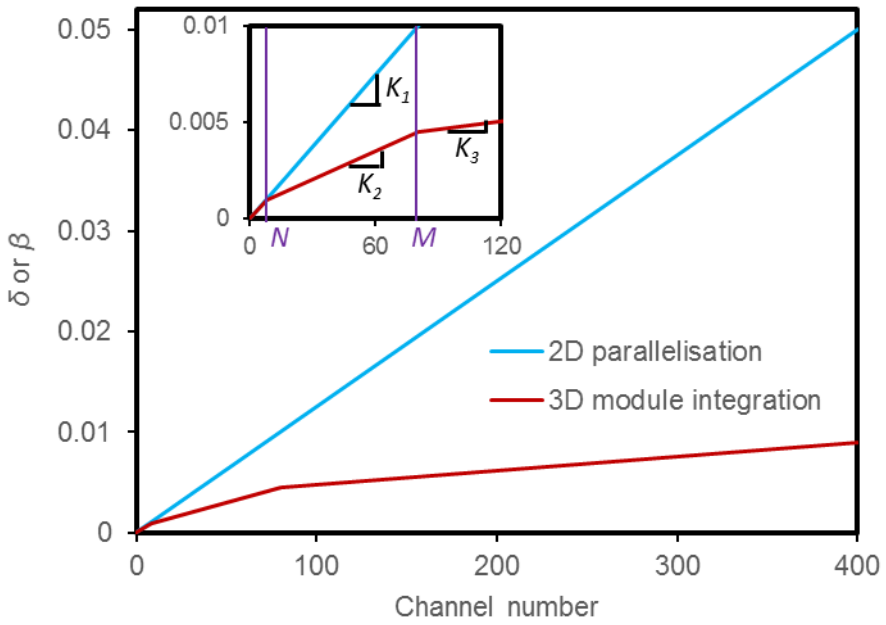

Fig. 5 Advantages of multi-dimensional scale-up strategy. δ or β is an indicator of product uniformity (*N*=8; *M*=10; *Q*=5).

3.2 Array-Level Characterization

Fig. 6 shows the experimental results for a parallel array with eight channels. The average diameters with corresponding CVs of droplets from the parallel array under different operating conditions are depicted. The results show that droplet size decreases with increase in the continuous phase flow rate while maintaining the dispersed phase flow rate at a constant value, as also reported in previous papers [22, 30]. For an individual channel, the monodispersity of droplets has a CV of 1.26% under a continuous phase flow rate of 1 mL/min and dispersed phase flow rate of 0.25 mL/min. The CVs for the array are much larger

(5%-7%), reflecting the existing challenges of up-scaling technology for microfluidics. For more details, Fig. 7a shows the droplet formation in a parallel array. Here, the flow rates of the dispersed and continuous phase are 2 mL/min and 8 mL/min, respectively, with an emulsion throughput of 600 mL/h. Then, the diameter histogram of droplets is obtained, yielding an average diameter of 951.81 μm with a CV of 5.28%. The polydispersity (CV = 5.28%) mainly results from the fluid distribution network. A photograph of the device used is shown in Fig. 7c. Under the same operating conditions, the experimental result of the circular array is shown in Fig. 6d-e. Compared to the parallel array, the generated droplets showed a narrower size distribution (CV = 3.04%), with a reduction by 42.4%. It is also noted that the average sizes of droplets generated in parallel array and circular array are slightly different, due to the different flow distribution performances, leading to different two-phase ratio (Qc/Qd) between the two arrangements.

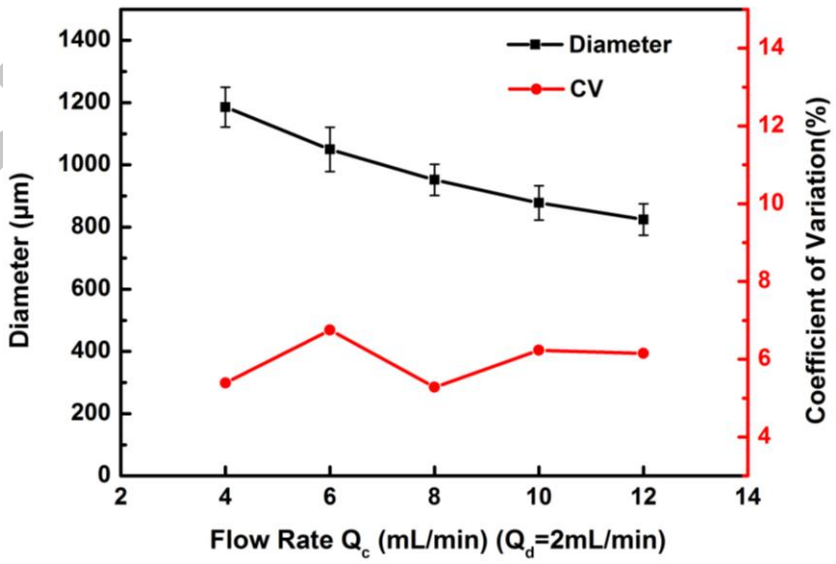

Fig. 6 Array-level characterization. Droplet diameters and CVs from parallel array with eight channels under different conditions.

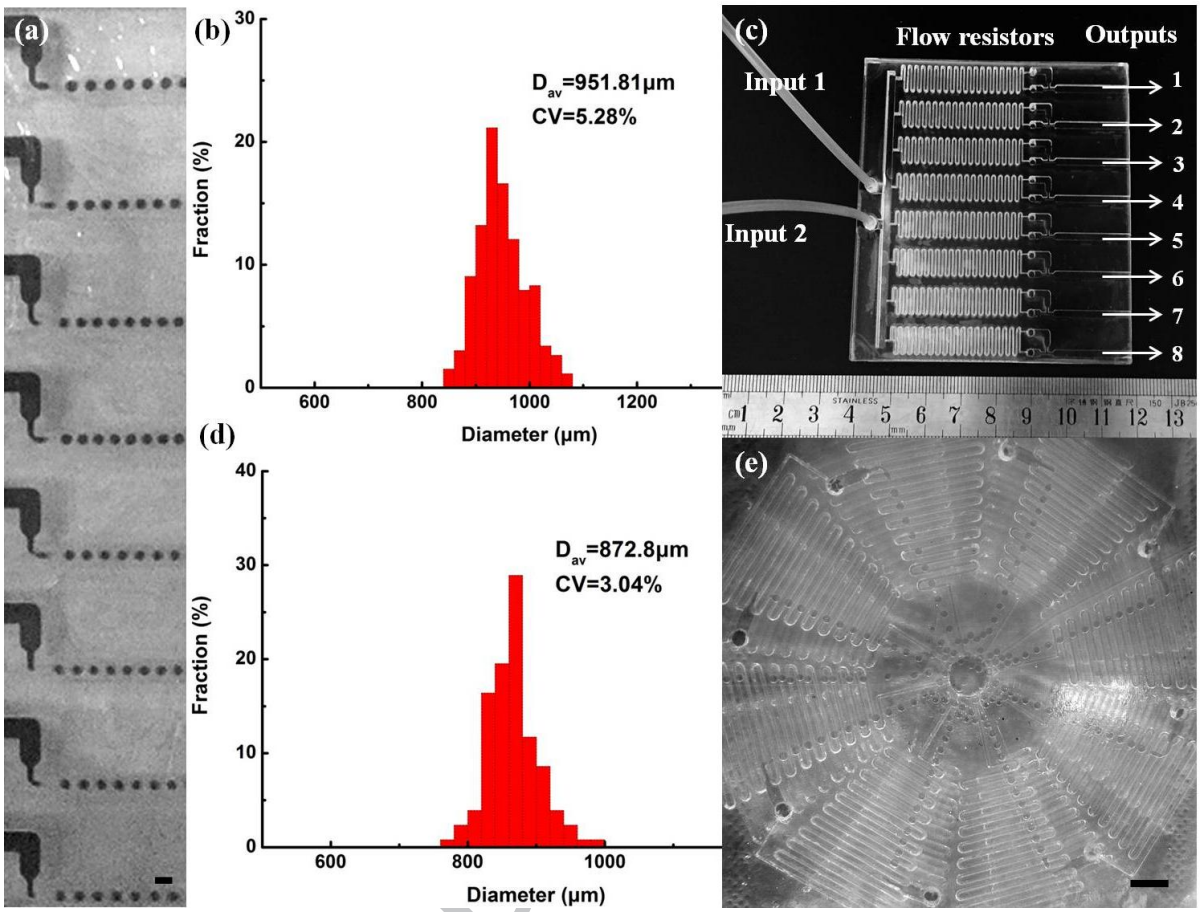

Fig. 7 Array Level Characterization. (a) Optical micrograph of formation of droplets in the parallel array. The scale bar is 2 mm. (b) Diameter histogram of droplets from the parallel array with an average diameter of 951.81 μm and a CV value of 5.28%. (c) A photograph of the experimental device of the parallel array. (d) Diameter histogram of droplets from the circular array with an average diameter of 872.8 μm and a CV value of 3.04%. (e) Optical micrograph of formation of droplets in the circular array. The scale bar is 5 mm.

Varieties of existing factors such as pump-induced fluctuation [31], random fabrication variations of the channel [32], and fabrication errors among array channels, as well as measurement uncertainty contribute to the polydispersity of droplets. For large-scale microfluidics, errors resulting from the fluid distribution network are more important to be

considered. The circular array results in a decreased R_f with a much lower δ compared to the parallel array, thereby achieving a higher distribution uniformity with a much lower CV value, as demonstrated by these comparative experiments.

3.3 Module-Level Characterization

The circular array is utilized for stacking because it shows better performance for the production of uniform droplets. Fig. 8 shows the stacking effect in a water/octane system and chitosan system. A different variation trend of the diameter of droplets affected by stacking appears for different fluid systems. For the water/octane system, under a dispersed phase of 20 mL/min and continuous phase of 80 mL/min, the droplet diameter shows an increasing variation ranging from 848.2 μm to 951.3 μm from the top to bottom array. The maximum error in droplet diameter among the ten arrays is 10.8% between the first and tenth arrays. The average diameter of droplets resulting from the module is 899.12 μm with a CV of 4.72% and a droplet throughput of 1.2 L/h. For the chitosan system, a smaller diameter and narrower distribution are obtained. The resulting microspheres present an average diameter of 539.65 μm and a CV of 3.59% from the module under a dispersed phase of 8 mL/min and continuous phase of 80 mL/min. The diameter histogram of droplets resulting from the two fluid systems is shown in Fig. 9b and Fig. 10c, respectively.

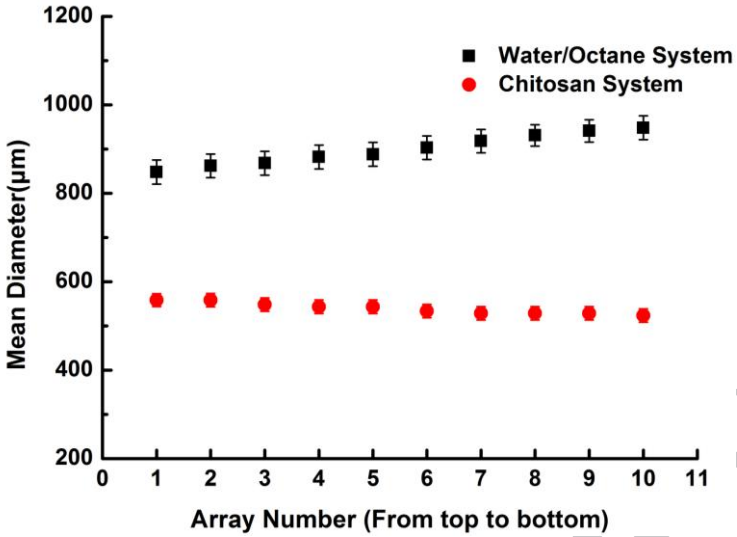

Fig. 8 Stacking effect of the module. Diameters from a module of ten arrays for the water/octane system and chitosan system. The first array refers to the top one.

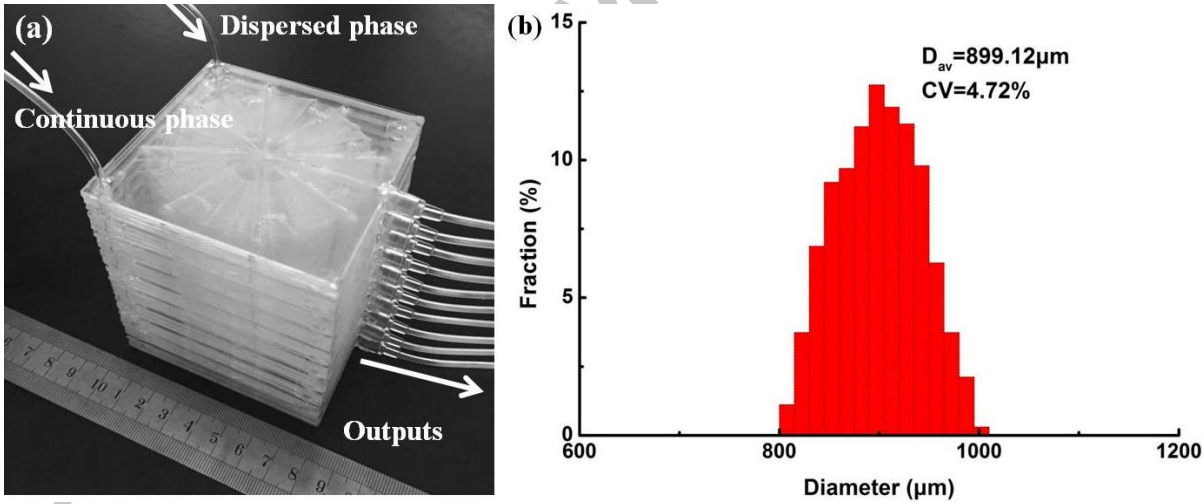

Fig. 9 Module-level characterization. (a) A photograph of the module. (b) Diameter histogram of droplets with an average diameter of 899.12 μm and a CV value of 4.72% for the water/octane fluid system. A video of droplet formation can be found in supporting information.

The combinational effect of flow resistance R_v and gravity motivation R_g dominates the

vertical distribution result (equation 4). In our module experiment, the two different fluid systems present entirely different results, demonstrating our stacking theory. For the water/octane system with a significantly low viscosity, gravity motivation R_g plays a more important role, causing increasing flow rates at the bottom array than at the top array. Therefore, a lower Q_c/Q_d value is obtained at the bottom array, which increases the size of droplets. In contrast, for the Chitosan system, the viscosity of the 2% Chitosan solution is 500 mPa·s, which is approximately 500 times that of water. Herein, the flow resistance R_v dominates the vertical flow distribution, resulting in greater flow toward the top array with a lower Q_c/Q_d, presenting an entirely different variation trend. Theoretically, the complete counteraction of R_v and R_g could yield a perfectly uniform distribution, and it is determined by fluid viscosity, vertical channel size, and operational condition. Further investigation of the mechanism of vertical distribution is needed for the optimization of device design.

3.4 System-Level Characterization

Obviously, several microfluidic modules could be integrated to build the microfluidic system to achieve a magnitude-order enhancement of throughput. Therefore, module integration is the third procedure of the scale-up strategy. Five microfluidic modules were integrated to build the microfluidic system to achieve a droplet throughput five times that of a single module. The operating results of five modules are listed in Table 1 with a continuous phase flow rate of 80 mL/min and dispersed phase flow rate of 20 mL/min for each module. The results indicate that slight differences in droplet diameter and size distribution exist among the five modules. The whole microfluidic system fabricated droplets with a CV of

6.98%. During the large-scale process, the uniformity of droplets worsens from the individual channel (CV = 1.26%) to circular array (CV = 3.04%) to stack module (CV = 4.72%) to the final system (CV = 6.98%), reflecting the existing challenge of drop-microfluidics up-scaling technology. In addition, the parallelization of more channels, the stacking of more arrays, and even the integration of more modules can be incorporated for further scale-up to feasibly achieve several to tens of tons of droplets per day.

Table 1 Operation results of the microfluidic system

Module Number	Average Diameter	CV
1	899.12 μm	4.72%
2	905.42 μm	5.02%
3	874.67 μm	5.46%
4	893.41 μm	4.81%
5	895.68 μm	4.72%
Microfluidic system	893.66 μm	6.98%

3.5 Chitosan/TiO_2 composite material characterization

Here, the as-developed module has been used to synthesize novel functional materials with a large production volume. Fig. 10 shows the characterization of the Chitosan/TiO_2 composite material produced by a module with a total of 80 channels. The chitosan/TiO_2 composite microspheres have an average diameter of 539.65 μm and a CV of 3.59% under dispersed and continuous phases estimated as 8 mL/min and 80 mL/min, respectively.

The decolourization performance of same amount (5 mg) of TiO_2 powder, chitosan microspheres, and chitosan/TiO_2 composite microspheres is depicted in Fig 10d. The results illustrate that nano-TiO_2 alone for methyl-orange photocatalytic treatment exhibits a lower decolourization rate and poor adsorption performance. Compared to single-component chitosan microspheres, the newly designed chitosan/TiO_2 composite microspheres exhibit a higher decolourization rate in the same period of time. After the saturated decolourization, chitosan/TiO_2 composite microspheres exhibit a higher removed efficiency of 65.3%, with an increase of 10.8% compared to single-component microspheres (η_t = 58.9%). The synergies of adsorption and photocatalytic degradation of chitosan/TiO_2 composite microspheres strengthen the decolourization performances for methyl-orange dye.

In our previous study [22], the same chitosan microspheres were prepared in an individual flow-focusing microchannel and tested for decolourization of dye solutions. Very similar adsorption performance was reported. It can be found that the up-scaling module presented in this study is capable to improve the functional material throughput while maintaining the similar performance.

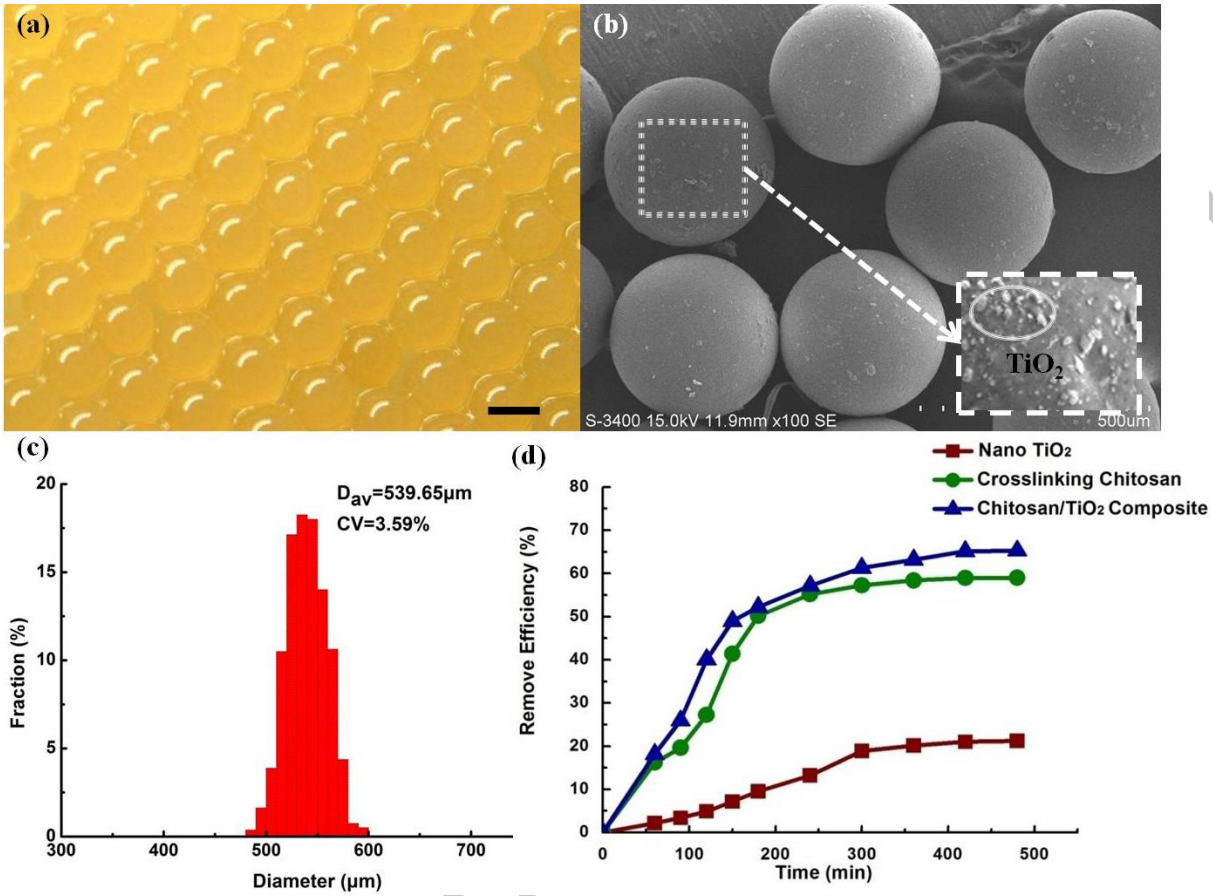

Fig. 10 Characterization of chitosan/TiO_2 composite material. Optical micrograph of the composite microspheres. Scale bar represents 500 μm. (b) SEM image of composite microspheres and TiO_2 distribution. (c) Diameter histogram of composite microspheres with an average diameter of 539.65 μm and a CV value of 3.59%. (d) Decolourization performance of chitosan/TiO_2 composite microspheres, together with nano-TiO_2 and chitosan microspheres.

4 Conclusions

A multi-dimensional scale-up strategy combining parallelization, stacking, and integration is developed to achieve the throughput enhancement of microfluidics and microreactors from the level of lab-on-chip to factory-on-chip, enabling the introduction of

microfluidic-based material synthesis technology to the chemical industry. A large scale 400-microchannel high-throughput system was demonstrated to make the factory-on-chip concept possible.

Parallelization and the stacking effect were investigated and discussed. Fluid-distribution imbalance is a major contributor to the polydispersity of droplets. Under the same operation conditions, a circular array (CV = 3.04%) reduced the CV value by 42.4% compared to a parallel array (CV = 5.28%) because its configuration facilitates more uniform fluid delivery resulting from a smaller pressure imbalance among inputs from neighbouring channels. Array stacking in the vertical direction caused the stacking effect dominated by the combinational effect of flow resistance and gravity motivation determined by fluid type, channel size, and operating condition. For the water/octane system with lower viscosity, the dominant effect of gravity caused an increasing droplet diameter from top to bottom. For the chitosan fluid system with a much higher viscosity, an entirely opposite trend was obtained.

In addition, the developed microfluidics module was applied to the synthesis of chitosan/TiO_2 composite material in a large volume. The functional material combines adsorption and photocatalytic degradation to strengthen the adsorption performance for methyl-orange dye. The novel material exhibits a higher removed efficiency of 65.3% with an increase of 10.8% compared to single-component chitosan microspheres of η_t = 58.9%. Above all, this work provides a great possibility for the further development of industrialization of microfluidic technology.

Acknowledgements

This work is supported by the research grant (No. 16DZ2260600) from Science and Technology Commission of Shanghai Municipality, the Fundamental Research Funds for the Central Universities (222201717012, 222201718005) and The Global Innovation Initiatives Award (S-ECAGD-13-CA-149 (DT)).

References

[1] XJ Yao, Y Zhang, LY Du, JH Liu and JF Yao, Review of the applications of microreactors, *Renewable and sustainable energy reviews*, 47(2015) 519-539.

[2] G. M. Whitesides, The origins and the future of microfluidics, *Nature*, 442(2006) 368-373.

[3] T Nisisako, T Torii, and T Higuchi. Novel microreactors for functional polymer beads. *Chemical Engineering Journal*, 101(2004) 23-29.

[4] S. Q. Xu, Z. H. Nie, M. Seo, P. Lewis, E. Kumacheva, H. A. Stone, P. Garstecki, D. B. Weibel, I. Gitlin, and G. M. Whitesides, Generation of monodisperse particles by using microfluidics: control over size, shape, and composition, *Angew. Chem. Int. Ed.*, 44(2005) 724-728.

[5] J. -T. Wang, J. Wang, and J. -J. Han, Fabrication of advanced particles and particle-based materials assisted by droplet-based microfluidics, *Small*, 7(2011)1728-1754.

[6] J. H. Kim, T. Y. Jeon, T. M. Choi, T. S. Shim, S. -H. Kim, and S. -M. Yang, Droplet microfluidics for producing functional microparticles, *Langmuir*, 30(2014) 1473-1488.

[7] W. Wang, M. -J. Zhang, and L. -Y Chu, Functional polymeric microparticles engineered from controllable microfluidic emulsions, *Accounts of chemical research*, 47(2014) 373-384.

[8] E. Campos, J. Branquinho, A. S. Carreira, A. Carvalho, P. Coimbra, P. Ferreira, and M. H. Gil, Designing polymeric microparticles for biomedical and industrial application, *European Polymer Journal*, 49(2013)2005-2021.

[9] C. Holtze, Large-scale droplet production in microfluidic devices-an industrial perspective, *J. Phys. D: Appl. Phys.*, 46(2013) 114008.

[10] T. Nisisako and T. Torii, Microfluidic large-scale integration on a chip for mass production of monodisperse droplets and particles, *Lab Chip*, 8(2008)287-293.

[11] W. Li, J. Greener, D. Voicu and E. Kumacheva, Multiple modular microfluidic (M3) reactors for the synthesis of polymer particles, *Lab Chip*, 9(2009)2715-2721.

[12] T. Nisisako, T. Ando and T. Hatsuzawa, High-volume production of single and compound emulsions in a microfluidic parallelization arrangement coupled with coaxial annular world-to-chip interfaces, *Lab Chip*, 12(2012)3426-3435.

[13] M. B. Romanowsky, A. R. Abate, A. Rotem, C. Holtze and D. A. Weitz, High throughput production of single core double emulsions in a parallelized microfluidic device, *Lab Chip*, 12(2012) 802-807.

[14] M. K. Mulligan and J. P. Rothstein, Scale-up and control of droplet production in coupled microfluidic flow-focusing geometries, *Microfluid Nanofluid*, 13(2012) 65-73.

[15] M. Muluneh and D. Issadore, Hybrid soft-lithography/laser machined microchip for the parallel generation of droplets, *Lab Chip*, 13(2013) 4750-4754.

[16] D. Conchouso, D. Castro, S. A. Khan and I. G. Foulds, Three-dimensional parallelization of microfluidic droplet generators for a litre per hour volume production of single emulsions, *Lab Chip*, 14(2014) 3011-3020.

[17] H. -H. Jeong, V. R. Yelleswarapu, S. Yadavali, D. Issadore and D. Lee, Kilo-scale droplet generation in three-dimensional monolithic elastomer device (3D MED), *Lab Chip*, 15(2015) 4387-4392.

[18] T. Femmer, A. Jans, R. Eswein, N. Anwar, M. Moeller, M. Wessling, and A. J.C. Kuehne, High-throughput generation of emulsions and microgels in parallelized microfluidic drop-makers prepared by rapid prototyping, *ACS Appl. Mater. Interfaces*, 7(2015) 12635-12638.

[19] A M. Nightingale, J H. Bannock, S H. Krishnadasan, F T. F. O'Mahony, S A. Haque, J Sloan, C Drury, R Mclntyre, and J C. de Mello, Large-scale synthesis of nanocrystals in a multichannel droplet reactor, *J. Mater. Chem. A*, 1(2013):4067-4076

[20] M. N. V. Ravi Kumar, A review of chitin and chitosan application, *React. Funct. Polym*, 46(2000)1-27.

[21] H. Zhao, X. M. Xu, J. H. Xu, T. Wang, G. S. Luo, Research process in microfluidic preparation of Chitosan functional material, *CIESC Journal*, 67(2016)373-378.

[22] Z. Dong, H. Xu, Z. S. Bai, H. Z. Wang, L. Zhang, X. J. Luo, Z. Y. Tang, R. Luque and J. Xuan, Microfluidic synthesis of high-performance monodispersed chitosan microparticles for methyl orange adsorption, *RSC Adv.*, 5(2015) 78352-78360.

[23] T. Aarthi and G. Madras, Photocatalytic degradation of rhodamine dyes with nano-TiO_2, *Ind. Eng. Chem. Res*., 46(2007) 7-14.

[24] Q. Li, H. J. Su, T. W. Tan, Synthesis of ion-imprinted chitosan-TiO_2 adsorbent and its multi-functional performances, *Biochem Eng J*., 38(2008) 212-218.

[25] C. E. Zubieta, P. V. Messina, C. Luengo, M. Dennehy, O. Pieroni, P. C. Schulz, Reactive

dyes remotion by porous TiO2-chitosan materials, *J Hazard Mater.*, 152(2008) 765-777.

[26] H Z Wang, S J Gu, D Y. C. Leung, H Xu, M K.H. L, L Zhang, J Xuan, Development and characteristics of a membraneless microfluidic fuel cell array, Electrochimica Acta, 135(2014)467-477

[27] N.L. Jeon, S.K.W. Dertinger, D.T. Chiu, I.S. Choi, A.D. Stroock, G.M. Whitesides, Generation of solution and surface gradients using microfluidic systems, Langmuir, 16(2000)8311

[28] C. Kim, K. Lee, J.H. Kim, K.S.Shin, K.J. Lee, T.Y. Kang, A serial dilution microfluidic device using a ladder network generating logarithmic or linear concentrations, Lab Chip, 8(2008)473

[29] K.W. Oh, K Lee, B. Ahn, E.P. Furlani, Design of pressure-driven microfluidic networks using electric circuit analogy, *Lab Chip*, 12(2012)515

[30] S Takeuchi, P Garstecki, D B Weibel, An axisymmetric flow-focusing microfluidic device, *advanced materials*, 17(2005)1067-1072

[31] Z. Li, S. Y. Mak, A. Sauret and H. C. Shum, Syringe-pump-induced fluctuation in all-aqueous microfluidic system implications for flow rate accuracy, *Lab chip*, 14(2014) 744-749.

[32] G. Tetradis-Meris, D. Rossetti, C. P. d. Torres, R. Cao, G. P. Lian, and R. Janes, Novel parallel integration of microfluidic device network for emulsion formation, *Ind. Eng. Chem. Res.*, 48(2009) 8881-8889.